Efficient blue organic light-emitting diodes using newly-developed pyrene-based electron transport materials

ARTICLE *in* ORGANIC ELECTRONICS · FEBRUARY 2009

Impact Factor: 3.83 · DOI: 10.1016/j.orgel.2008.10.015

3 AUTHORS, INCLUDING:

Changhee Lee
Seoul National University
293 PUBLICATIONS **4,004** CITATIONS

Organic Electronics 10 (2009) 163–169

Contents lists available at ScienceDirect

Organic Electronics

journal homepage: www.elsevier.com/locate/orgel

Efficient blue organic light-emitting diodes using newly-developed pyrene-based electron transport materials

Hyoung-Yun Oh [a], Changhee Lee [b], Seonghoon Lee [a,*]

[a] Molecular Electronics and NanoStructures Lab, School of Chemistry, Seoul National University, Shilim-dong, San 56-1, Seoul 151-747, Republic of Korea
[b] School of Electrical Engineering and Computer Science, Seoul National University, Gwanak, P.O. Box 34, Seoul 151-600, Republic of Korea

ARTICLE INFO

Article history:
Received 6 September 2008
Received in revised form 24 October 2008
Accepted 25 October 2008
Available online 5 November 2008

PACS:
42.70.−a
85.60.Jb
42.70.Jk
81.05.Lg

Keywords:
Blue OLED
Degradation
Pyrene-based electron transport material

ABSTRACT

We synthesized new kinds of pyrene-based electron transport materials: 1,6-di(pyridin-3-yl)-3,8-di(naphthalen-1-yl)pyrene (N1PP) and 1,6-di(pyridin-3-yl)-3,8-di(naphthalen-2-yl)pyrene (N2PP). The external quantum efficiencies of the device with these electron transport materials increase by more than 50% at 1 mA cm^{-2} compared with those of the device with representative Alq_3 as an electron transport material. The enhanced quantum efficiency is due to a balanced charge recombination in an emissive layer. Electron mobilities in N1PP and N2PP films are three times higher than that in Alq_3. Highly enhanced power efficiency is achieved due to a low electron injection barrier and a high electron mobility. We find that the luminance degradation in the blue OLEDs is correlated with the HOMO energy levels of electron transport materials.

1. Introduction

Since the first report on light emission from double-layered OLEDs by Tang and Van Slyke [1], advances in luminescent RGB materials, device structures, and manufacturing processes have led to the demonstration of full-color OLED displays that are capable of showing video rate images. There are still obstacles for the commercialization of full-color OLED displays. Among them, development of highly efficient blue emitters with sufficient operational stability should be made. Substantial performance enhancement can be achieved through synthesizing new blue luminescent organic materials by way of rational design of the photoactive chemical structure. A phosphorescent (triplet emission) blue electroluminescence (EL) with a high external quantum efficiency and a saturated blue color has been thought to be an alternative but its instability problems remain unresolved [2–4]. Another approach to achieve maximum device efficiency is to balance charge carrier recombination, because the hole mobility in the OLED is usually much higher than the electron mobility under the same electric field [5,6]. And thus, emitting and charge-transporting materials with a high ionization potential value such as oxadiazole [7], benzimidazole [8], diarylsilole group materials [9] and electron transport materials [10,11] were synthesized and applied to OLEDs. The lifetimes of the devices made with these electron transport materials (ETMs) are short compared with those of the devices using a small molecule Alq_3. There are needs to develop emitting and charge-transporting materials with a longer lifetime and to understand the degradation mechanism. The increased luminance efficiency and the understanding of luminance degradation in OLEDs will be keys to the use of OLED technology in the next generation flat displays and light sources. Here, we report the development of the new kinds of ETMs based on

* Corresponding author. Tel.: +82 2 880 1456; fax: +82 2 889 1568.
E-mail address: shnlee@snu.ac.kr (S. Lee).

1566-1199/$ - see front matter © 2008 Elsevier B.V. All rights reserved.
doi:10.1016/j.orgel.2008.10.015

pyrene molecules and the measurement of the lifetime of ETMS and find the luminance degradation process of the blue OLEDs.

2. Experimental

2.1. Materials

Dibromo pyrene and 3-pyridinyl boronic acid were purchased from SFC Co. Ltd. All other reagents and solvents were purchased from Aldrich Chemical Co. and Fluka. Those were used as received. For absorption and emission experiments, spectroscopic grade CH_2Cl_2 (Aldrich) was used.

2.1.1. 1,6-Di(pyridin-3-yl)-pyrene

To a solid mixture of 1,6 dibromo-pyrene (7.2 g, 20 mmol) and 3-pyridinyl boronic acid (7.4 g, 60 mmol) were added a solution of 70 ml tetrahydrofuran (THF) and 10 ml toluene. After 60 ml of 2 M aqueous potassium carbonate was added to the mixture, it was degassed by bubbling nitrogen for 30 min. Finally, 0.6 mmol of tetrakis(tri-phenylphosphine)palladium ($Pd(Ph_3)_4$) was added to the mixture. The mixture was vigorously refluxed under nitrogen for 24 h. When the reaction mixture was cooled down to room temperature, it was poured into 200 ml methanol. After filtering it off, the crude solid was re-precipitated from chloroform and methanol. Light-yellow powder (5.3 g, 74%) was more purified by flash chromatography with chloroform. mp 249 °C. δ_H (500 MHz; $CDCl_3$; Me_4Si) 8.88 (2H, s), 8.73 (2H, d, *J* 3.5), 8.27 (2H, d, *J* 7.7), 8.15 (4H, m), 7.97 (4H, m), 7.52 (2H, m). Elemental analysis: Found: C, 87.27%; H, 4.35%; N, 7.97%; Calc. for $C_{26}H_{16}N_2$: C, 87.62%; H, 4.52%; N, 7.86%; M^+, 357.

2.1.2. 1,6-Di(pyridin-3-yl)-3,8-dibromo-pyrene

Pyridinium hydrobromide perbromide (7.97 g, 25 mmol) was added to a solution of 1,6-di(pyridin-3-yl)-pyrene (3.56 g, 10 mmol) in 1,2 dichlorobenzene (200 ml). The mixture was refluxed for 12 h. After cooling, 100 ml of methanol was slowly added and the precipitate was filtered. Pure product (3.6 g, 70%) was obtained from re-precipitation with pyridine and methanol. mp: 378 °C. δ_H (500 MHz; $CDCl_3$; Me_4Si) 8.89 (2H, s), 8.79 (2H, d, *J* 5.0), 8.50 (2H, d, *J* 9.5), 8.3 (2H, s), 8.16 (2H, d, *J* 10.0), 7.95 (2H, d, *J* 10.0), 7.54 (2H, m). Elemental analysis: Found: C, 60.93%; H, 2.90%; N, 5.67%; Calc. for $C_{26}H_{14}Br_2N_2$: C, 60.73%; H, 2.74%; N, 5.45%; M^+, 515.

2.1.3. 1,6-Di(pyridin-3-yl)-3,8-di(naphthalen-1-yl)pyrene (N1PP)

To a solid mixture of 1,6-di(pyridin-3-yl)-3,8-dibromo-pyrene (5.1 g, 10 mmol) and 1-naphthyl boronic acid (4.3 g, 25 mmol) were added a solution of 70 ml tetrahydrofuran (THF) and 10 ml toluene. After 60 ml of 2 M aqueous potassium carbonate was added to the mixture, it was degassed by bubbling nitrogen for 30 min. Finally, 0.05 mmol of tetrakis(tri-phenylphosphine)palladium ($Pd(Ph_3)_4$) was added to the mixture. The mixture was vigorously refluxed under nitrogen for 24 h. When the reaction mixture was cooled down to room temperature, it was poured into 200 ml methanol. After filtering it off, the crude solid was re-precipitated from chloroform and methanol. Light-yellow powder (4.9 g, 80%) was more purified by flash chromatography with chloroform. mp 377 °C. δ_H (500 MHz; $CDCl_3$; Me_4Si) 8.91 (2H, s), 8.66 (2H, d, *J* 4.0), 8.05 (2H, s), 8.03 (2H, d, *J* 7.9), 7.99 (2H, t, *J* 3.9), 7.96 (4H, m), 7.75 (2H, d, *J* 7.9), 7.65 (4H, m), 7.50 (2H, t), 7.46 (2H, d, *J* 7.0), 7.40 (2H, m), 7.32 (2H, t). Elemental analysis: Found C, 90.74%; H, 4.66%; N, 4.53%; Calc. for $C_{46}H_{28}N_2$: C, 90.76%; H, 4.64%; N, 4.60%; M^+, 609.

2.1.4. 1,6-Di(pyridin-3-yl)-3,8-di(naphthalen-2-yl)pyrene (N2PP)

Synthetic procedure is the same as in N1PP, except using 2-naphthyl boronic acid instead of 1-naphthyl boronic acid. Yellow powder (4.8 g, 80%), mp 340 °C. δ_H (500 MHz; $CDCl_3$; Me_4Si) 8.96 (2H, s), 8.72 (2H, d, *J* 4), 8.28 (2H, d, *J* 8.0), 8.14 (6H, m), 8.05 (4H, m), 7.94 (4H, m), 7.80 (2H, d, *J* 7.0), 7.59 (4H, m), 7.51 (2H, m). Elemental analysis: Found: C, 90.74%; H, 4.61%; N, 4.45%; Calc. for $C_{46}H_{28}N_2$: C, 90.76%; H, 4.64%; N, 4.60%. M^+, 609.

2.2. Instrument

2.2.1. Solution electrochemistry and UV–vis spectroscopy

Cyclic voltammetry was performed in 0.5 mM solution of the compounds with a Potentiostat & Galvanistat (EG&G Princeton Applied Research, Model 273A). All oxidation measurements were carried out in nitrogen-purged anhydrous CH_2Cl_2 containing 0.1 M tetraethyl ammonium tetrafluoroborate (Et_4NBF_4, Aldrich) as a supporting electrolyte. Platinum disk (2 mm in diameter), platinum wire, and Ag/AgCl (saturated) were used as the working, counter, and reference electrodes, respectively. The voltage between the working and counter electrodes was swept at a scan rate of 50 mV s^{-1}. The potentials for all the materials were the traced to the first anodic peak by using a differential pulse mode. Absorption spectra of 10^{-5} M solution of the samples were collected using a spectrophotometer (SCINCO UVS2100). The optical bandgap was determined from the absorption onset of that spectrum.

2.2.2. OLED fabrication

Patterned indium tin oxide (ITO)-coated glass substrates (NHT, 2 mm × 2 mm, 20 Ω cm^{-2}) were thoroughly cleaned, treated with oxygen plasma (150 W, 5 min, 4×10^{-2} torr). Organic materials were purified by train-sublimation method prior to device experiments. OLEDs were prepared in multiple-source thermal evaporation system at a base pressure of 3×10^{-6} torr or lower. The deposition rate, which is controlled using a deposition controller (Inficone IC/5), was 2 Å s^{-1} for organic materials, except for dopants which were co-evaporated at an appropriate rate to obtain the desired doping level. All the OLEDs were characterized by using a source-unit (Keithley 2400) and a spectroradiometer (Photo Research PR650). To determine the OLED lifetimes, the devices were driven at a constant DC current, while the emission

intensity was monitored using a silicon photodiode at room temperature.

2.2.3. Transient EL and PL

The ITO treatments and organic evaporating conditions are all the same as described in the OLED fabrication. The NPB (60 nm) as a HTL was coated on the ITO, and then electron transport materials (they also behave as emitting materials in this case, 85 nm) were coated on that. Al (100 nm) was used as a cathode. During measurement, a rectangular voltage pulse (amplitude 6–8 V, pulse duration time 3 μs) was applied to an OLED using a pulse generator (HP model 241B). The time-resolved EL from the OLED was measured by placing a miniature photomultiplier tube (PMT, Acton spectra pro 300i Hamamatsu Model 5783-02) directly on the top of the OLED. The output photocurrent from the PMT was sourced into a sensing resistor from which the transient EL signal can be displayed on a storage oscilloscope (Tektronix TDS 754B). The electron mobility was then calculated using $\mu = d/(\tau_d E)$, with d denoting the film thickness and E the applied field, assuming the field drops across the sample compound and neglecting the built-in potential. For the PL measurement, sample thin films (45 nm) were prepared on the ITO glass and Al (100 nm) was coated to protect the films from air. Fluorescence spectra upon excitation with 355 nm were collected by a PMT.

3. Results and discussion

The polycyclic aromatic hydrocarbons such as naphthalenes, anthracenes, and pyrenes, compared with other hetero-aromatic compounds, are known to be not suitable for ETMs because of their high reduction potentials, but they have good thermal stability and no absorption at longer wavelengths than 430 nm [12]. Among them, the pyrene has relatively high electron affinity values and better thermal stability [13]. Moreover, it has four possible positions for substitution reaction (1, 3, 6, and 8 positions), so we can introduce various kinds of functional groups to it to tailor the desired electrical and optical properties. To increase the electron affinity of pyrene-based aromatic hydrocarbons, we attached two 3-pyridyl moieties at the 1 and 6 positions. Additionally, in order to ensure morphologically stable amorphous film, we introduced two naphthyl moieties into 3 and 8 positions. Expecting the positional dependence of physical properties, we used 1-naphthyl boronic acid and 2-naphthyl boronic acid to synthesize 1,6-di(pyridin-3-yl)-3,8-di(naphthalen-1-yl)-pyrene (hereafter, N1PP) and 1,6-di(pyridin-3-yl)-3,8-di(naphthalen-2-yl)pyrene (hereafter, N2PP), respectively. Synthetic routes to the new ETMs (N1PP and N2PP) are shown in Scheme 1. (The detailed description is given in Section 2.)

The molecular structures of N1PP and N2PP were confirmed by ^{1}H NMR, mass spectrometry, and elemental analysis. Thermal properties of N1PP and N2PP were investigated by means of differential scanning calorimetry (DSC). A glass transition temperature (T_g) was obtained from the second heating scan of the glassy samples cooled after the first heating up to melting temperature (T_m). The heating rate was 10 °C min^{-1}. The T_m's of N1PP and N2PP appear at 377 and 337 °C, respectively, and N1PP shows 20 °C higher T_g than N2PP (shown in Table 1). Because the 1-naphthyl group is expected to be more properly oriented towards the pyrene backbone than the 2-naphthyl group is, N1PP molecule may form a more rigid structure where the intermolecular dipole interactions are favored [14,15]. The crystallization temperature (T_c) of N1PP was observed at 250 °C by the second heating, but no T_c of N2PP was found (Supplementary information), which indicates that N2PP has more glass-like property. However, T_g's of N1PP and N2PP are high enough to keep the amorphous films from being crystallized during the device operation.

The oxidation potentials for the compounds were measured by a differential pulse voltammetry and were used for the estimation of the highest occupied molecular orbital (HOMO) levels, based upon the known linear correla-

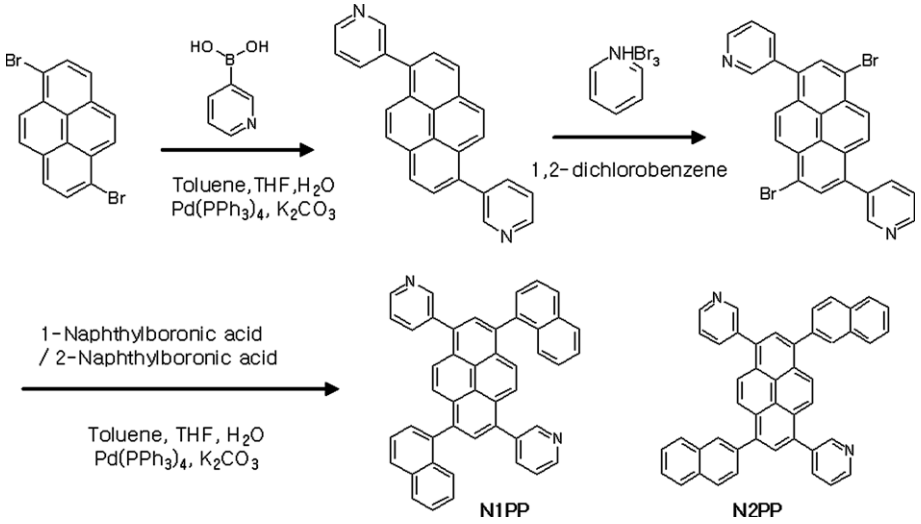

Scheme 1. Synthetic routes of N1PP and N2PP.

tion between the two parameters [16]. Because Alq_3, N1PP, and N2PP did not undergo reversible oxidation, the potentials given for these molecules are the first irreversible anodic peak potentials, which are considered as the half-wave oxidation potentials ($E^{OX}_{1/2}$). The anodic peak potential of ferrocene measured by a differential pulse voltammetry corresponded within 30 mV to its half-wave oxidation potential obtained from the anodic peak (E^{a}_{p}) and the cathodic peak potential (E^{c}_{p}). The bandgap energies were estimated from the onset of UV–vis absorption spectra in dilute solution (Supplementary information).

N2PP (Eg = 2.9 eV) has a smaller bandgap than N1PP (Eg = 3.0 eV). HOMO's and LUMO's of N1PP and N2PP are shown in Fig. 1. Furthermore, in order to get more detailed substituent positional effect, we calculated electronic energy of N1PP and N2PP, using the density functional theory (DFT) B3LYP/6-31G* level Spartan'06 program. Dihedral angles between a naphthyl unit and a pyrene backbone in N1PP and N2PP are and 73.6° and 54.5°, respectively, The conjugation between naphthalene moiety and pyrene moiety is more favourable in N2PP than in N1PP. N2PP shows more bathochromic shift of π–π^* transition as shown in Table 1. The two materials, however, show relatively higher oxidation potentials and larger bandgap energy than Alq_3, as shown in Table 1.

The blue OLEDs were fabricated by high-vacuum thermal evaporation of OLED materials onto ITO-coated glass that was used as the anode. All the devices, we fabricated have the same architectures as one shown in the left-half of Fig. 1, differing in the component of electron transport layer. We tested Alq_3, newly-synthesized N1PP and N2PP as electron transport layer (ETL) or electron transport material (ETM).

Firstly, a 60-nm-thick hole injection layer (HIL) consisting of 4,4'-bis[N-[4-{N,N-bis(3-methylphenyl)amino}-phenyl]-N-phenylamino]biphenyl (DNTPD) was deposited, and followed by a 30-nm-thick 4,4'-bis [N-(1-naphthyl)-N-phenylamino]biphenyl (NPB) as a hole transport layer (HTL). Secondly, a 25-nm-thick emissive material layer (EML) was formed by co-depositing 3 wt% of 2,5,8,11-tetra(tert-butyl)perylene (TBP) as a dopant and 9,10-di-(2-naphthyl)anthracene (ADN) as a host [17]. Finally, a 25-nm-thick electron transport layer (ETL) consisting of Alq_3 for device 1 (N1PP for device 2, N2PP for device 3) was deposited. LiF (0.5 nm) and Al (100 nm) worked as an electron injection facilitating a layer and a cathode

Table 1
Physical properties of electron transport materials (N1PP and N2PP) used in this work.

Compound	T_g [°C]	λ^{abs}_{max} [nm][b]	λ^{PL}_{max} [nm][c]	$E^{OX}_{1/2}$ [mV][d]	HOMO [eV][e]	Bandgap [eV][f]
$A1q_3$	175[a]	386	512	1140	5.51	2.80
N1PP	172	380	421	1570	6.14	3.03
N2PP	152	386	434	1320	5.79	2.94

[a] Literature value [15].
[b] 0.01 mM solutions in CH_2Cl_2.
[c] 0.01 mM solutions in CH_2Cl_2 upon excitation at 355 nm.
[d] The first irreversible anodic peak potential measured by a differential pulse voltammetry was considered as the half-wave oxidation potential ($E^{OX}_{1/2}$) (see Supplementary information).
[e] Estimated using a linear correlation by the measured anodic peak potential [16].
[f] Estimated from the absorption onset.

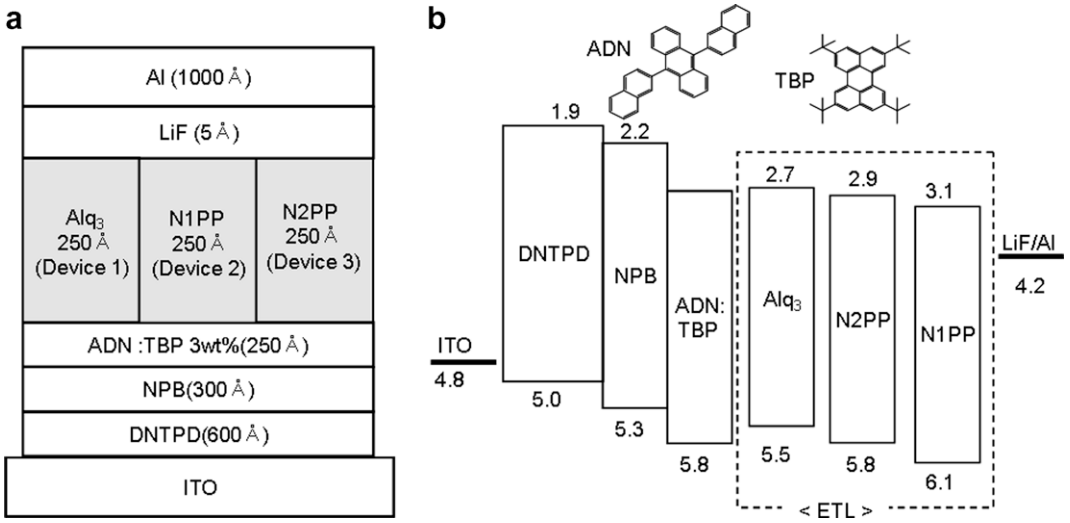

Fig. 1. (a) Device architecture for OLED, where ETM is Alq_3 for device 1, N1PP for device 2, and N2PP for device 3. (b) Energy diagram of multi layer devices; HOMO and LUMO levels of DNTPD, Alq_3, N1PP, and N2PP are estimated from the first oxidation potential and the absorption onset (Section 2). Those of NPB and ADN are previously reported values [22].

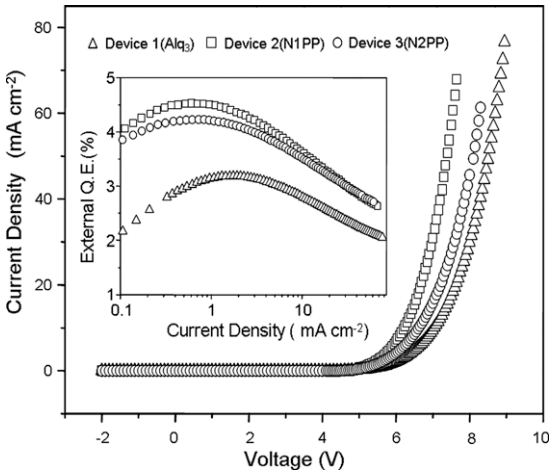

Fig. 2. The *J–V* (current–density–voltage) curves of blue devices based on different ETMs. The inset shows the external quantum efficiency as a function of current density.

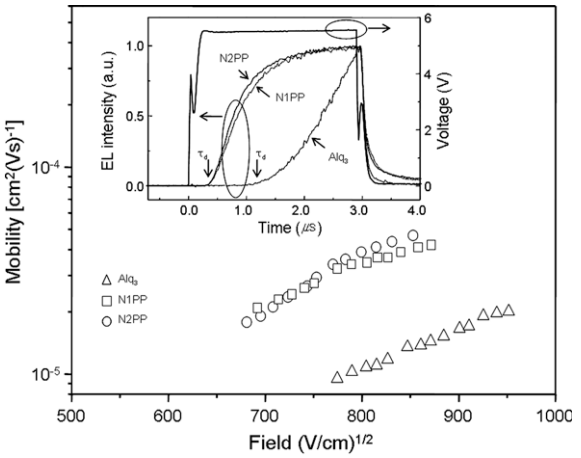

Fig. 3. The electron mobilities in Alq_3, N1PP, and N2PP are plotted as a function of the square-root of the electric field. Their transient electroluminescent signals around 5.5 V are also shown in the inset (more specifically, applied voltages for Alq_3, N1PP, and N2PP devices are 5.67 V, 5.52 V, and 5.45 V, respectively).

layer, respectively. Inside a glove box, all the devices were encapsulated by a 1-mm-thick glass cover containing a humidity absorber (Dynic). Devices 1, and 2, and 3 have Alq_3, N1PP, and N2PP as an electron transport layer (ETL), respectively.

The current density (*J*)–voltage (*V*)–luminescence (*L*) characteristics of the blue OLEDs with different ETLs were measured by source-measure-units (Keithley 2400) and a spectrometer (Photo research PR650). The *J–V* characteristics are shown in Fig. 2 and the external quantum efficiencies as a function of *J* are also shown in the inset of Fig. 2. Applying approximately 10 mA cm^{-2} to the devices, the driving voltages of the devices 1, 2, and 3 are 7.05 V (10.1 mA cm^{-2}), 6.25 V (10.4 mA cm^{-2}), and 6.65 V (10.4 mA cm^{-2}), respectively. The external quantum efficiencies of the devices are 2.8%, 3.6%, and 3.5%, respectively. The required operating voltage for 10 mA cm^{-2} is in the order of device 1 > device 3 > device 2, which corresponds to the height of the electron injection barrier estimated by the electrochemical data (Alq_3 > N2PP > N1PP shown in the right-half of Fig. 1, i.e. N1PP has the lowest injection barrier among them.).

Additionally, the external quantum efficiencies of the device with the newly-developed pyrene-based molecules as electron transport materials increase by more than 50% at 1 mA cm^{-2} compared with those of the device with Alq_3 as an electron transport material. This enhancement is due to the newly-developed pyrene-based molecules as electron transport materials through an improved electron mobility and a lower injection barrier. In order to confirm this fact, we fabricated three kinds of devices to measure the electron mobility by the transient electroluminescence (EL) with ITO/NPB (60 nm)/ETM (85 nm)/Al device structure, where ETM is Alq_3, N1PP, or N2PP (described in Section 2) [18]. The typical transient EL signals for the three devices are shown in the inset of Fig. 3, where the time delay (τ_d) of Alq_3 film is 1.1 μs and both N1PP and N2PP films have about 0.3 μs of τ_d around 5.5 V. We collect τ_d by varying the electric field. The electron mobility is plotted as a function of the square-root of the electric field and is given in Fig. 3. For the electric field at 0.7 MV cm^{-1}, the estimated electron mobility in Alq_3 film is 1.4×10^{-5} $cm^2\,(V\,s)^{-1}$ that is in a good agreement with the reported value, $10^{-6} \sim 10^{-5}$ $cm^2\,(V\,s)^{-1}$ [5,19]. Those in N1PP and

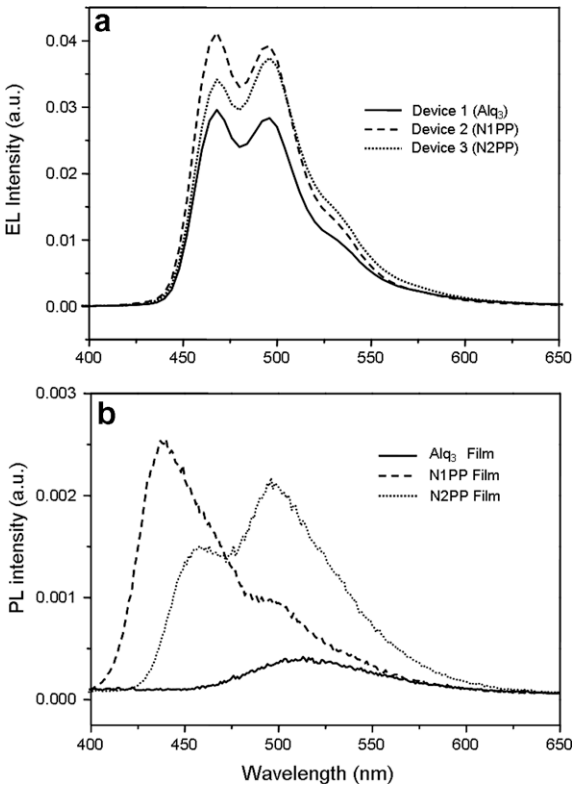

Fig. 4. (a) EL spectra of devices 1, 2, and 3 at $J = 10$ mA cm^{-2}. (b) Photoluminescence spectra of the vacuum-deposited amorphous thin films of Alq_3, N1PP and N2PP upon UV excitation at 355 nm.

N2PP films are 3.7×10^{-5} cm^2 (V s)$^{-1}$ and 4.3×10^{-5} cm^2 (V s)$^{-1}$, respectively. As expected, the electron mobilities in the newly-developed pyrene-based electron transport materials (N1PP and N2PP) turned out to be higher than that in better-known Alq_3, and thus enhanced the external quantum efficiency of devices 2 and 3 using N1PP and N2PP as ETLs which can be explained in terms of an efficient balanced carrier recombination in the emissive material layer (EML).

The EL spectra of the three devices at 10 mA cm^{-2} are also shown in Fig. 4a together with their PL spectra in Fig. 4b. The luminescences with 1931 Commission Internationale del' Eclairage (CIE) coordinates (x,y) of devices 1, 2, and 3 are 495 cd m^{-2} with (0.148, 0.294), 627 cd m^{-2} with (0.138, 0.276), and 672 cd m^{-2} with (0.148, 0.318), respectively. Device 2 (with N1PP as an ETL) emits the most saturated blue color and the intense peak at 468 nm. Device 3 (with N2PP as an ETL) shows a little bit broader spectrum and the intense peak centered at 496 nm. The difference in spectral feature among these results from the enhanced blue emission. Gathering from the PL data shown in Fig. 4b, the totally enhanced portion of blue emission in device 2 with N1PP as an ETL, compared with device 1 with Alq_3 as an ETL, comes from an improved carrier recombination in an EML due to the HOMO energy level of N1PP as a hole barrier and three times higher electron mobility of N1PP than that of Alq_3 If some of the enhanced portion of the blue emission in device 2 with N1PP as an ETL come from the blue emission of N1PP itself, then the blue emission around 430 nm should be shown in the EL spectrum of device 2. In fact, it is not shown in the EL spectrum of device 2 as given in Fig. 4a. On the other hand, the excimer peaks of pyrene [20] around 500 nm are generated from both N1PP and N2PP, but N2PP having more planar structure for easier formation of excimers shows much stronger excimer peak, for device 3 with N2PP as an ETL, considering that 9,10-di(2-naphthyl)anthracene (ADN) is so ambipolar [21] that the holes passing over it can reach the ETL of N2PP, some of the enhanced portion of blue emission can be originated from N2PP and its excimer themselves.

With the newly-developed pyrene-based molecules (N1PP and N2PP) as an ETL, we get the enhanced blue emission due to 3 times higher electron mobility in those and the HOMO levels of those, compared with Alq_3 as an ETL. More specifically, the totally enhanced portion of the blue emission with N1PP as an ETL originates from the HOMO energy level of N1PP as a hole barrier and three times higher electron mobility, while some of the enhanced portion of the blue emission with N2PP as an ETL results from an improved carrier recombination at EML due to three times higher electron mobility and the others come from the blue emission of N2PP and its excimer themselves. We have performed an accelerated lifetime test at 2000 cd m^{-2} initial brightness for the three devices. Applied current and voltage are 52.8 mA cm^{-2} and 8.55 V for the device 1, 42.2 mA cm^{-2} and 7.25 V for device 2, and 37.3 mA cm^{-2} and 7.80 V for the device 3. The accelerated test data are given in Fig. 5. The operation times of 40% light emission reduction occurring for devices 1, 2, and 3 are 620 h, 87 h, and 517 h, respectively.

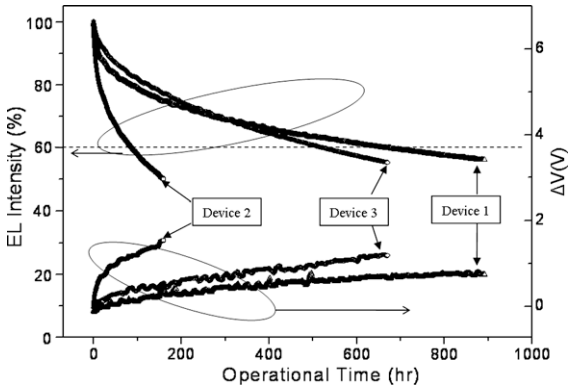

Fig. 5. Luminance deteriorations and drive voltage variation curves (ΔV) of the devices as a function of time at 2000 cd m^{-2}.

Interestingly, the lifetime of the device 2 with N1PP is shortened by a factor of 5, compared with device 3 with N2PP, even though the only difference in the two structures is the substituent (1-naphthyl or 2-naphthyl). This observation gives some light on the device degradation. According to the energy levels of each material shown in Fig. 1b, device 2 with N1PP as an electron transport layer has a hole injection barrier between an emissive material layer (EML) and an electron transport layer (ETL), but device 3 with N2PP as an ETL does not have a hole injection barrier. The holes in device 3 (with no hole injection barrier) can penetrate the ETL layer deeply and spread over larger area and disappear away with electrons than those in device 2 with N1PP as an ETL. The hole accumulation caused by a hole injection barrier accelerate the material decomposition through a higher concentration of ionized carbocation species in the emissive materials layer [22–24]. Compared to Alq_3 and N2PP, N1PP has the highest hole injection barrier. And thus the device 2 with N1PP as an ETM degrades faster than the others. Usually, the deterioration of the light emission is observed in company with an increase in the drive voltage. The drive voltage variations, ΔV's of devices 1, 2, and 3 at 40% light emission reduction, are 0.68 V, 1.2 V, and 1.0 V, respectively. The highest drive voltage increase (ΔV = 1.2 V) is also observed in the device 2 with N1PP as an ETL, with which we can suppose that the voltage increase during the lighting process has a strong correlation with some degradation at the interface between EML and ETL as well. The luminance degradation in the blue OLEDs was correlated with the HOMO energy levels of electron transport materials. Based upon the fact that N1PP and N2PP have 3 times higher mobility than Alq_3 and the understanding on the device degradation with N1PP and N2PP, further works on the better devices with a longer lifetime are in progress.

4. Conclusions

In conclusion, we synthesized new kinds of pyrene-based electron transport materials: 1,6-di(pyridin-3-yl)-3,8-di(naphthalen-1-yl)pyrene (N1PP) and 1,6-di(pyridin-3-yl)-3,8-di(naphthalen-2-yl)pyrene (N2PP). The external

quantum efficiencies of the device with the newly-developed pyrene-based molecules as electron transport materials increase by more than 50% at 1 mA cm^{-2} compared with those of the device with representative Alq_3 as an electron transport material. The enhanced quantum efficiency is due to the balanced charge recombination in an emissive layer. Electron mobilities in N1PP and N2PP films are 3.7×10^{-5} $cm^2 (V s)^{-1}$ and 4.3×10^{-5} $cm^2 (V s)^{-1}$, respectively. These values are three times higher than that of Alq_3. Highly enhanced power efficiency (e.g., 1.4 lm W^{-1} for device 1 with Alq_3, 2.0 lm W^{-1} for device 2 with N1PP, and 2.1 lm W^{-1} for device 3 with N2PP at 2000 cd m^{-2}) is achieved due to a low electron injection barrier and a high electron mobility. We find that the luminance degradation in the blue OLEDs is correlated with the HOMO energy levels of electron transport materials.

Acknowledgements

This work was supported in part by MOE through BK21 program and Seoul R&BD program. We thank KOSEF and CNNC for supporting this research. We also acknowledge the student support from the Korea Science and Engineering Foundation through NanoSystems Institute – National Core Research Center.

Appendix A. Supplementary data

Supplementary data associated with this article can be found, in the online version, at doi:10.1016/j.orgel.2008.10.015.

References

[1] C.W. Tang, S.A. Van Slyke, Appl. Phys. Lett. 51 (1987) 913.
[2] R.J. Holmes, B.W. D'Andrade, S.R. Forrest, X. Ren, J. Li, M.E. Thompson, Appl. Phys. Lett. 83 (2003) 3818.
[3] S.-J. Yeh, M.-F. Wu, C.-T. Chen, Y.-H. Song, Y. Chi, M.-H. Ho, S.-F. Hsu, C.H. Chen, Adv. Mater. 17 (2005) 285.
[4] X. Ren, J. Li, R.J. Holmes, P.I. Djurovich, S.R. Forrest, M.E. Thompson, Chem. Mater. 16 (2004) 4743.
[5] B.J. Chen, W.Y. Lai, Z.Q. Gao, C.S. Lee, S.T. Lee, W.A. Gambling, Appl. Phys. Lett. 75 (1999) 4010.
[6] T.-Y. Chu, O.-K. Song, Appl. Phys. Lett. 90 (2007) 203512.
[7] S. Tokito, H. Tanaka, N. Koda, A. Okada, Y. Tago, Macromol. Symp. 125 (1997) 181.
[8] J. Shi, C.W. Tang, C.H. Chen, US Patent 5646948, 1997.
[9] M. Uchida, T. Izumizawa, T. Nakano, S. Yamaguchi, K. Tamao, K. Furukawa, Chem. Mater. 13 (2001) 2680.
[10] A.P. Kulkarni, C.J. Tonzola, A. Babel, S.A. Jenekhe, Chem. Mater. 16 (2004) 4556.
[11] P. Strohriegl, J.V. Grazulevicius, Adv. Mater. 14 (2002) 1439.
[12] C.J. Tonzola, M.M. Alam, W. Kaminsky, S.A. Jenekhe, J. Am. Chem. Soc. 125 (2003) 13548.
[13] R.S. Becker, W.E. Wentworth, J. Am. Chem. Soc. 85 (1963) 2210.
[14] D.E. Loy, B.E. Koene, M.E. Thompson, Adv. Funct. Mater. 12 (2002) 245.
[15] K. Naito, A. Miura, J. Phys. Chem. 97 (1993) 6240.
[16] B.W. D'Andrade, S. Datta, S.R. Forrest, P. Djurovich, E. Polikarpov, M.E. Thompson, Org. Electron. 6 (2005) 11.
[17] J. Shi, C.W. Tang, Appl. Phys. Lett. 80 (2002) 3201.
[18] C. Hosokawa, H. Tokailin, H. Higashi, T. Kusumoto, Appl. Phys. Lett. 60 (1992) 1221.
[19] S.C. Tse, H.H. Fong, S.K. So, J. Appl. Phys. 94 (2003) 2033.
[20] (a) T. Forster, K. Kasper, Z. Physik Chem. N.F. 1 (1954) 275;
(b) N.J. Turro, in: Modern Molecular Photochemistry, Univ. Science Books, Mill Valley, California, 1991 (Ch. 5).
[21] S.C. Tse, S.K. So, M.Y. Yeung, C.F. Lo, S.W. Wen, C.H. Chen, Chem. Phys. Lett. 353 (2002) 407.
[22] S.W. Culligan, A.C.-A. Chen, J.U. Wallance, K.P. Klubek, C.W. Tang, S.H. Chen, Adv. Funct. Mater. 16 (2006) 1481.
[23] H. Aziz, Z.D. Popovic, N.X. Hu, A. Hor, G. Xu, Science 283 (1999) 1900.
[24] Y.C. Luo, H. Aziz, G. Xu, Z.D. Popovic, Chem. Mater. 19 (2007) 2079.